Development of a Semi-Analytic Nodal Method with Edge Segmented for Two-Dimensional Triangular Geometry

Junwoo Lee[a], Yonghee Kim[a*]
Nuclear and Quantum Engineering, Korea Advanced Institute of Science and Technology (KAIST)
291 Daehak-ro, Yuseong-gu, Daejeon 34141, Republic of Korea
**Corresponding author: yongheekim@kaist.ac.kr*

Keywords : Semi-Analytic Nodal Method (SANM), Edge segmentation, Two-dimensional, Triangular geometry

1. Introduction

Hexagonal-lattice cores are attracting attention in small modular reactor (SMR) designs for their favorable neutron economy [1], and many nodal codes have been developed, from hexagon-based methods such as HOPEN [2], AFEN [3,4], the refined AFEN [5] and ANC-H [6,7] to methods employing a triangular expansion such as TPEN [8], TRIPEN [9], A-SANM [10] and ABFEM-T [11], and EFEN [12] for unstructured meshes.

Among the constraints determining the intranodal flux, the corner-point flux remains the most widely adopted, retained even in recent semi-analytic formulations, where three of twelve nodal unknowns are assigned to it [10]. Although it provides a strong constraint, obtaining it requires a separate global sparse linear system for each energy group at non-negligible cost, with no consistent way of determining it at boundaries [9]. Furthermore, unlike the edge-based discontinuity factor derived from the conservation conditions of nodal equivalence theory [13], a vertex has zero measure and carries neither a reaction rate nor a net current, so that no equivalence condition follows.

Corner-free formulations exist, but each is restricted: the refined AFEN method needs additional moment unknowns and a singularity-removal procedure reported only for rectangular and hexagonal geometries [5]. Kim and Cho's half-interface averaged flux formulation addresses a mixed R–Z mesh and two groups [14]. ABFEM-T is limited to the homogeneous Helmholtz form of the two-group equation [11] and EFEN assumes a flat source [12].

Motivated by these considerations, the Semi-analytic Edge-segmented Nodal method for TRIangular geometry (SENTRI) was developed by combining segmented partial currents with a SANM kernel and a cubic source on a triangular lattice. SENTRI uses six half-edge segmented partial incoming currents as the only interface constraints. The source is expanded into a cubic polynomial, while the intranodal flux is represented using both polynomial basis function and SANM-based hyperbolic to capture steep spatial gradients. The resulting one-node kernel solves the nodal problem locally on a single triangle and is verified against the VVER-1000 and VVER-440 2D benchmarks [6,7].

2. Methodology

2.1 Governing Equation and Node Definition

The governing equation solved in SENTRI(Semi-analytic Edge-segmented Nodal method for TRIangular geometry) is given by Eq. (1).

$$-D_g\nabla^2\phi_g(x,y)+\Sigma_{r,g}\phi_g(x,y)=\sum_{g'=1}^{G}\left[(1-\delta_{g,g'})\Sigma_{s,g'\to g}+\frac{\chi_g}{k_{eff}}\nu\Sigma_{f,g'}\right]\phi_{g'}(x,y)+L_g^z(x,y). \quad (1)$$

The Eq. (1) is two-dimensional neutron multigroup diffusion equation. The axial transverse leakage term, $L_g^z(x,y)$, is omitted, as it is beyond the scope of the present study. In SENTRI, two types of equilateral triangles with side length h, namely upward and downward triangles, are employed as the basic nodal elements, as shown in Fig. 1. The corresponding coordinate systems are defined in Eq. (2).

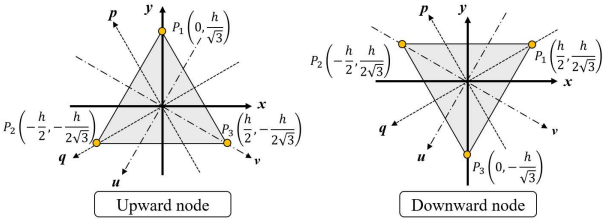


Fig. 1. Node definition in SENTRI

$$\begin{bmatrix}p\\q\end{bmatrix}=\begin{bmatrix}-\frac{1}{2} & \frac{\sqrt{3}}{2}\\ -\frac{\sqrt{3}}{2} & -\frac{1}{2}\end{bmatrix}\begin{bmatrix}x\\y\end{bmatrix},\qquad \begin{bmatrix}u\\v\end{bmatrix}=\begin{bmatrix}-\frac{1}{2} & -\frac{\sqrt{3}}{2}\\ \frac{\sqrt{3}}{2} & -\frac{1}{2}\end{bmatrix}\begin{bmatrix}x\\y\end{bmatrix}. \quad (2)$$

2.2 Edge-Segmented Partial Currents

SENTRI employs partial currents defined on the half-edge segments of each triangular side to replace the corner-point flux. The edge segments *v1*, *v2*, *q1*, *q2*, *y1*, and *y2* are defined with respect to the direction vectors normal to each edge, as shown in Fig. 2. The partial currents are then defined based on the P_1 approximation, with the positive direction taken outward from the node. In particular, the partial currents associated with *y1* are defined by Eq. (3).

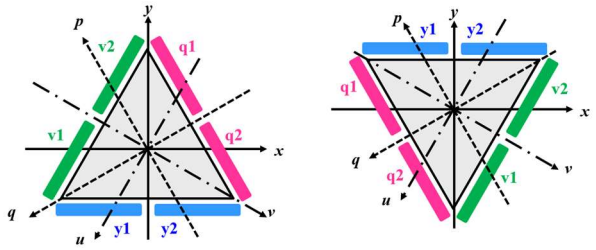


Fig. 2. Half-edge segments of each triangular side

$$\begin{cases} \bar{J}^{in}_{g,y1} = \dfrac{2}{h}\displaystyle\int_{-\frac{h}{2}}^{0} dx \left[\frac{df_{g,y1}}{4}\phi_g(x,y) + \frac{D_g}{2}\nabla_{-y}\phi_g(x,y)\right]. \\ \bar{J}^{out}_{g,y1} = \dfrac{2}{h}\displaystyle\int_{-\frac{h}{2}}^{0} dx \left[\frac{df_{g,y1}}{4}\phi_g(x,y) - \frac{D_g}{2}\nabla_{-y}\phi_g(x,y)\right]. \end{cases} \quad (3)$$

Consequently, six incoming partial and six outgoing partial currents are defined per node.

2.3 Basis Functions and Intranodal Flux

Based on the SANM, Eq. (1) can be rewritten as Eq. (4), with the source term defined in Eq. (5)-1,2.

$$\nabla^2\phi_g(x,y) - \kappa_g^2\phi_g(x,y) = -\frac{1}{D}Q_g(x,y), \qquad \kappa_g^2 = \frac{\Sigma_{r,g}}{D_g} \quad (4)$$

$$Q_g(x,y) = \sum_{g'=1}^{G}\left[(1-\delta_{g,g'})\Sigma_{s,g'\to g} + \frac{\chi_g}{k_{eff}}\nu\Sigma_{f,g'}\right]\phi_{g'}(x,y). \quad (5)-1$$

$$Q_g(x,y) \cong \sum_{n=0}^{8} q_{g,n}\varphi_n(x,y). \quad (5)-2$$

The intranodal flux — the general solution of Eq. (4) — is the sum of a homogeneous and a particular part, as in Eq. (6): hyperbolic functions for the former and polynomials for the latter.

$$\phi_g(x,y) = \phi_g^H(x,y) + \phi_g^P(x,y). \quad (6)$$

Unlike TPEN, TRIPEN, and A-SANM, SENTRI builds them along the edge-tangential direction (x, u, p). Since the segmentation splits each edge along its tangent, a normal-varying function contributes equally to both half-edges and cannot distinguish them, whereas the odd-order tangential terms (x^3, u^3, p^3) break this left–right symmetry and keep the six segmented partial currents linearly independent. The intranodal flux is therefore defined as in Eq.(7), (8), and Table 1.

$$\phi_g^H(x,y) = \sum_{n=0}^{5} a_{g,n}e^{\kappa_g(x\cos\theta_n + y\sin\theta_n)}, \qquad \theta_n = \frac{n\pi}{3}. \quad (7)$$

$$\phi_g^P(x,y) = \sum_{n=0}^{8} c_{g,n}\varphi_n(x,y). \quad (8)$$

Table I. Polynomial Basis Functions

$\varphi_0(x,y)$	1	$\varphi_5(x,y)$	p^2
$\varphi_1(x,y)$	x	$\varphi_6(x,y)$	x^3
$\varphi_2(x,y)$	y	$\varphi_7(x,y)$	u^3
$\varphi_3(x,y)$	x^2	$\varphi_8(x,y)$	p^3
$\varphi_4(x,y)$	u^2		

2.4 Source Expansion

Within the SANM framework, the source term is approximated by a cubic polynomial, which requires the general solution – a combination of hyperbolic and polynomial functions – to be recast into a polynomial form, $\hat{\phi}(x,y)$, as shown in Eq. (9).

$$\phi_g^H(x,y) + \phi_g^P(x,y) \cong \hat{\phi}(x,y) \equiv \sum_{i=0}^{8} b_{g,i}\varphi_i(x,y) \quad (9)$$

$$\iint_{\partial\Omega} d\Omega\, \varphi_n(x,y)\left[\phi_g^H(x,y) + \phi_g^P(x,y) - \hat{\phi}(x,y)\right] = 0. \quad (10)$$

Several closure schemes were examined. The adopted scheme preserves the six half-edge averaged surface fluxes and determines the remaining three coefficients by the weighted residual method (WRM), Eq. (10), with the $\varphi_n(x,y)$ with n = 0,1,2 were used as the weighting functions.

2.5 Nodal Balance and Node-Averaged Flux

For each energy group, the node-averaged flux is obtained from the decoupled nodal balance equation, Eq. (11), in which the six edge-segmented net surface currents constitute the leakage term.

$$\frac{2}{h\sqrt{3}}\sum_{k=v,q,y}\left(\bar{J}^{out}_{g,k1} - \bar{J}^{in}_{g,k1} + \bar{J}^{out}_{g,k2} - \bar{J}^{in}_{g,k2}\right) + \Sigma_{r,g}\bar{\phi}_g = \bar{Q}_g,$$

$$where, \qquad \bar{Q}_g = q_{g,0} + \frac{h^2}{24}(q_{g,3} + q_{g,4} + q_{g,5}). \quad (11)$$

$$\bar{\phi}_g = \frac{16\sinh^2\left(\frac{h\kappa}{4}\right)}{h^2\kappa^2}(a_{g,1} + a_{g,5}) + c_{g,0} + \frac{h^2}{24}(c_{g,3} + c_{g,4} + c_{g,5}). \quad (12)$$

Integrating the intranodal flux over the node then gives the node-average flux, Eq. (12), as a linear combination of the integrated hyperbolic and polynomial terms.

2.6 Solution Algorithm

For a given node and energy group, the neutron flux is expressed as a linear combination of fifteen basis functions with their coefficients. Among these, the nine coefficients of the particular solution are determined uniquely once the source expansion coefficients are specified, as given by Eqs. (13)-(16).

$$c_{g,0} = \frac{q_{g,0}}{\Sigma_{r,g}} + \frac{2D_g}{\Sigma_{r,g}^2}(q_{g,3} + q_{g,4} + q_{g,5}). \quad (13)$$

$$c_{g,1} = \frac{q_{g,1}}{\Sigma_{r,g}} + \frac{3D_g}{\Sigma_{r,g}^2}(2q_{g,6} - q_{g,7} - q_{g,8}). \quad (14)$$

$$c_{g,2} = \frac{q_{g,2}}{\Sigma_{r,g}} + \frac{3\sqrt{3}D_g}{\Sigma_{r,g}^2}(-q_{g,7} + q_{g,8}). \quad (15)$$

$$c_{g,n} = \frac{q_{g,n}}{\Sigma_{r,g}}(n \geq 3). \quad (16)$$

The remaining six unknowns are then determined by six constraints, for which the six edge-segmented partial

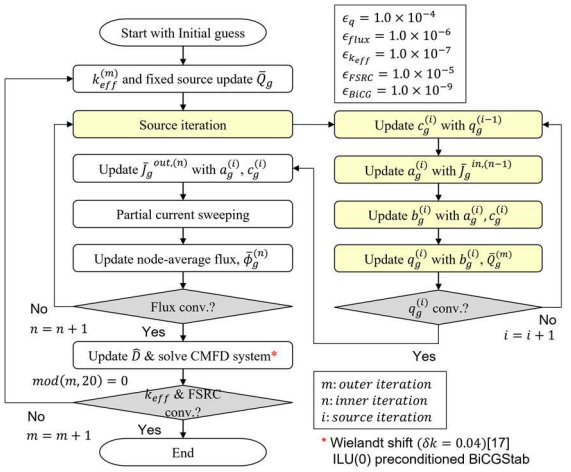


Fig. 3. Flow chart of SENTRI

incoming currents are used. Essentially, SENTRI is based on a one-node kernel that takes the incoming partial currents as input, produces the outgoing partial currents as output, and computes the node-average flux, performing partial-current sweeping with the adjacent nodes until convergence.

The overall calculation procedure is shown in Fig. 3. The inner iteration, which converges the flux, is carried out by the one-node kernel, while a conventional outer iteration updates and checks the convergence of the multiplication factor and the fission source.

Convergence of the source iteration, the inner iteration, and the fission source (FSRC) was judged by the relative L2-norm error, with thresholds of 1.0×10^{-4}, 1.0×10^{-6}, and 1.0×10^{-5}, respectively. For the k_{eff}, a relative error of 1.0×10^{-7} was used as the convergence criterion.

3. Numerical Results

The method was verified on VVER-440 and VVER-1000 two-dimensional benchmark problems[7]. The boundary condition was specified as albedo(α) defined as the ratio of the net surface current to the surface flux. The results were compared against existing codes in terms of the multiplication factor and the RMS, mean absolute, and maximum errors of the power distribution.

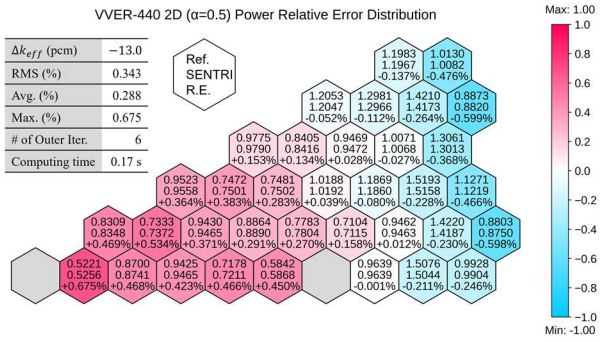


Fig. 4. Results of VVER-440 ($\boldsymbol{\alpha = 0.5}$) **problem**

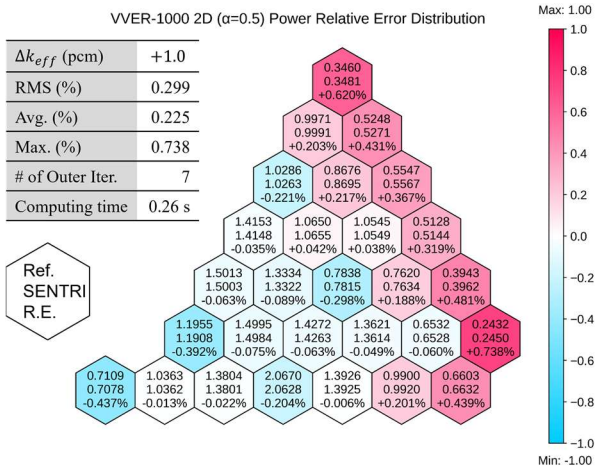


Fig. 5. Results of VVER-1000 ($\boldsymbol{\alpha = 0.5}$) **problem**

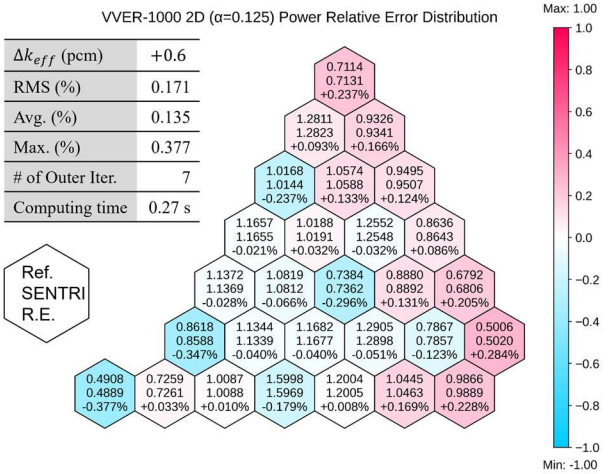


Fig. 6. Results of VVER-1000 ($\boldsymbol{\alpha = 0.125}$) **problem**

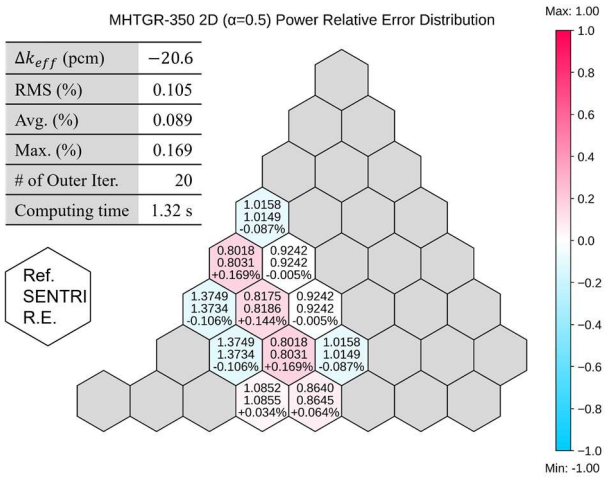


Fig. 7. Results of MHTGR-350[16] ($\boldsymbol{\alpha = 0.5}$) **problem**
(Δk against the FVM reference)

In addition, the Wielandt shift was applied in all calculations with δk = 0.04 [17], and the CMFD linear system was solved by ILU(0)-preconditioned BiCGSTAB. All calculations were run on an Intel Xeon Silver 4210R processor with 20 OpenMP threads. The performance of the method for multigroup problems was

evaluated on the 10-group MHTGR-350 problem [16]. The reference power distribution was obtained by Richardson extrapolation of FVM solutions with 1,536 and 6,144 triangles per hexagon.

Table II. Summary of results for the benchmark problems

Problem	Solver	Δk_{eff} (pcm)	Max Abs. Err.(%)	Avg. Rel. Err.(%)
VVER -440 α = 0.5	TRIPEN	3	0.39	0.16
	TPEN	0	0.34	0.14
	HOPEN	13	0.61	0.29
	ANC-H	29	1.20	-
	AFEN	23	1.25	0.52
	EFEN	-47	1.92	-
	A-SANM*	33	-	-
	SENTRI	**-13**	**0.68**	**0.29**
VVER -1000 α = 0.5	TRIPEN	-7	0.26	0.12
	TPEN	-15	0.99	0.28
	HOPEN	30	3.84	1.52
	ANC-H	4	1.20	-
	AFEN	32	3.73	1.52
	ABFEM-T	1	0.49	0.15
	A-SANM*	28	-	-
	SENTRI	**1**	**0.74**	**0.23**
VVER -1000 α = 0.125	TRIPEN	-19	1.20	0.30
	TPEN	-15	0.90	0.20
	HOPEN	22	1.25	0.66
	ANC-H	9	0.50	-
	AFEN	22	1.20	0.60
	ABFEM-T	-2	0.31	0.13
	SENTRI	**1**	**0.38**	**0.14**
MHTGR -350 α = 0.5	AFEN[16]	-23	-	-
	SENTRI	**-21**	**0.17**	**0.09**

* Not reported against the FDM reference [7],[10]

For a fair comparison, the average errors were evaluated for the solvers that provide results for all three benchmark problems, as shown in Fig. 8.

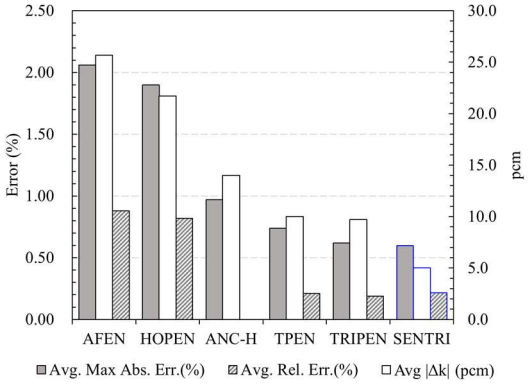


Fig. 8. Comparison of average errors over the three benchmark problems

The average relative power error of ANC-H is not available in the original reference [7][9] and is therefore left blank.

4. Conclusions and Future Works

A triangular-node SANM formulation employing half-edge segmented partial currents in place of the corner-point flux has been developed and verified against the VVER-440, VVER-1000, and MHTGR-350 bench-marks. As shown in Fig. 8, it achieved the smallest average multiplication-factor error among the codes reporting all three VVER problems, with power-distribution errors comparable to TPEN and TRIPEN.

First, in the VVER-440 problem SENTRI outperformed EFEN at a comparable mesh of about six triangles per hexagon (13 vs. 47 pcm, 0.68 vs. 1.92 % maximum power error). Since both employ segmented partial currents, this isolates the limitation of the flat-source assumption, which EFEN offsets only with about twice as many nodes. Second, whereas the maximum power error of TRIPEN increased 4.6-fold, from 0.26 % at α = 0.5 to 1.20 % at α = 0.125, that of SENTRI decreased from 0.74 % to 0.38 %. This is attributed to the boundary-layer representation of the hyperbolic basis and an interface treatment independent of the corner-point balance. Third, SENTRI gave smaller multiplication-factor errors than A-SANM against the same reference solutions (13 vs. 33 pcm and 1 vs. 28 pcm), showing that semi-analytic accuracy is attainable without the corner-point flux. The same kernel extended directly to the 10-group MHTGR-350 problem, with −20 pcm against CAPP (refined AFEN: −23 pcm) and a maximum block-power error of 0.17 %.

The nonlinear CMFD acceleration was further improved by a Wielandt shift with an all-group coupled CMFD solve. With identical results, this reduced the outer iterations from 11 to 6 for VVER-440 and from 31 to 20 for MHTGR-350, and the computing time by 24–43 %.

Future work will extend the method to three dimensions, optimize the nodal kernel, which now dominates the computing time, and quantify the gain from removing the corner-point balance. Discontinuity factors defined on the segmented interfaces will also be generated from transport solutions, to confirm that practical core analysis is achievable without the corner-point flux and its accompanying discontinuity factors.

ACKNOWLEDGEMENTS

This research was supported by Korea Energy Technology Evaluation and Planning (KETEP) grant funded by the Korean Government (MCEE) (RS-2024-00439210).

REFERENCES

[1] Black, G., Shropshire, D., Araújo, R., van Heek, A., 2023. "Prospects for nuclear microreactors: A review of the technology, economics, and regulatory considerations." *Nuclear Technology* **209**(sup1), S1–S20.

[2] Cho, J.Y., Kim, C.H., 1998. "Higher order polynomial expansion nodal method for hexagonal core neutronics analysis." *Annals of Nuclear Energy* **25**(13), 1021–1031.

[3] Noh, J.M., Cho, N.Z., 1994. "A new approach of analytic basis function expansion to neutron diffusion nodal calculation." *Nuclear Science and Engineering* **116**(3), 165–180.
[4] Cho, N.Z., Noh, J.M., 1995. "Analytic function expansion nodal method for hexagonal geometry." *Nuclear Science and Engineering* **121**(2), 245–253.
[5] Woo, S.W., Cho, N.Z., Noh, J.M., 2001. "The analytic function expansion nodal method refined with transverse gradient basis functions and interface flux moments." *Nuclear Science and Engineering* **139**(2), 156–173.
[6] Chao, Y.A., Tsoulfanidis, N., 1995. "Conformal mapping and hexagonal nodal methods—I: Mathematical foundation." *Nuclear Science and Engineering* **121**(2), 202–209.
[7] Chao, Y.A., Shatilla, Y.A., 1995. "Conformal mapping and hexagonal nodal methods—II: Implementation in the ANC-H code." *Nuclear Science and Engineering* **121**(2), 210–225.
[8] Cho, J.Y., Joo, H.G., Cho, B.O., Zee, S.Q., 2001. "Hexagonal CMFD formulation employing triangle-based polynomial expansion nodal kernel." *Proc. M&C 2001*, Salt Lake City, UT, USA.
[9] Kochunas, B., Seker, V., Ward, A., 2024. "Triangular polynomial expansion nodal method in AGREE." *Annals of Nuclear Energy* **206**, 110632.
[10] Jang, J., Lee, D., 2024. "Development and verification of multigroup advanced semi analytic nodal method solver for HTGR analysis with MHTGR-350." *Annals of Nuclear Energy* **209**, 110818.
[11] Wang, K., Wu, H., Cao, L., Wang, C., 2010. "Analytic basis function expansion nodal method for neutron diffusion equations in triangular geometry." *Proc. ICONE18*, Xi'an, China.
[12] Li, Y., Wu, H., Cao, L., 2013. "Unstructured triangular nodal-SP3 method based on an exponential function expansion." *Nuclear Science and Engineering* **174**(2), 163–171.
[13] Smith, K.S., 1986. "Assembly homogenization techniques for light water reactor analysis." *Progress in Nuclear Energy* **17**(3), 303–335.
[14] Kim, D.S., Cho, N.Z., 2003. "The analytic function expansion nodal (AFEN) method with half-interface averaged fluxes in mixed geometry nodes for analysis of pebble bed modular reactor (PBMR) cores." *Journal of Nuclear Science and Technology* **40**(5), 291–297.
[15] Cho, J.Y., Lee, H.C., Song, J.S., 2015. "DeCART equivalent group constants generation for hexagonal TPEN method." *Proc. RPHA15*, Jeju, Korea.
[16] Noh, J.M., 2020. "A response matrix method for the refined analytic function expansion nodal (AFEN) method in the two-dimensional hexagonal geometry and its numerical performance." *Nuclear Engineering and Technology* **52**, 2422–2430.
[17] Downar, T., Xu, Y., Seker, V., Hudson, N., 2009. "Theory manual for the PARCS kinetics core simulator module." University of Michigan, Ann Arbor, MI, USA.